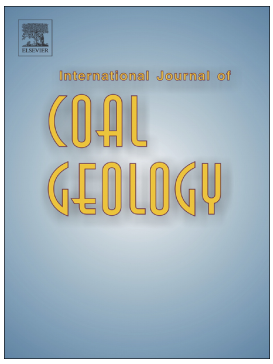

Insights into matrix compressibility of coals by mercury intrusion porosimetry and N2 adsorption

Qian Li, Yidong Cai, Dameng Liu, Yingfang Zhou, Dawei Lv

PII: S0166-5162(18)30525-1
DOI: https://doi.org/10.1016/j.coal.2018.11.007
Reference: COGEL 3116

To appear in: *International Journal of Coal Geology*

Received date: 29 May 2018
Revised date: 6 October 2018
Accepted date: 8 November 2018

Please cite this article as: Qian Li, Yidong Cai, Dameng Liu, Yingfang Zhou, Dawei Lv , Insights into matrix compressibility of coals by mercury intrusion porosimetry and N2 adsorption. Cogel (2018), https://doi.org/10.1016/j.coal.2018.11.007

Insights into matrix compressibility of coals by mercury intrusion porosimetry and N_2 adsorption

Qian Li[a], Yidong Cai[a,b*], Dameng Liu[a], Yingfang Zhou[c], Dawei Lv[b]

[a]Coal Reservoir Laboratory of National Engineering Research Center of CBM Development & Utilization, School of Energy Resources, China University of Geosciences, Beijing 100083, China

[b]Shandong Provincial Key Laboratory of Depositional Mineralization & Sedimentary Minerals, Shandong University of Science and Technology, Qingdao, Shandong 266590, China

[c]King's College, University of Aberdeen, Aberdeen, AB24 3UE, United Kingdom

* Corresponding author, Email: yidong.cai@cugb.edu.cn

Abstract

Matrix compressibility and pore properties (pore size distribution) of a rank range of coals was investigated using mercury intrusion porosimetry (MIP) on coal cores with the pore size distribution also being determined using low temperature at 77 K nitrogen adsorption/desorption isotherms for crushed samples. The coal matrix compressibility is significant when the pressure of MIP is from 0.0074-35 MPa. Mathematical models were developed (based on MIP and nitrogen adsorption/desorption isotherms) to establish the porosity/pore size distribution relationships with matrix compressibility. For coal ranks, the matrix compressibility was between 0.24×10^{-4} to 13.56×10^{-4} MPa^{-1}, and had a negative exponential relationship with the vitrinite reflectance ($R_{o,m}$%). Lignites have the maximum matrix compressibility due to their structural open structure having limitied compaction during coalification. In addition to the pore structure relationship the composition, moisture, and ash yields impacts on compressibility were also examined. Inertinite-rich coals however had a low matrix compressibility across the rank range, which may be due to the interinhibitive relationships between the mesopores, macropores and minerals. The wetting action of high moisture (water molecules) weakens the link between the coal particles of the lignites and the subbituminous coals, which causes abnormally high compressibility. Observations here relate to hydrofracturing or CO_2 injection behaviors during enhancing coalbed methane (CBM) recovery.

Keywords: coals; matrix compressibility; mercury intrusion porosimetry; low-temperature nitrogen adsorption

1. Introduction

The decrease in fluid pressure during coalbed methane (CBM) production results in volume changes of both reservoir fluids and coal reservoirs (Liu and Harpalani, 2014). The volumetric response to these pressure changes (Palmer and Mansoori, 1998; Pan et al., 2010) and/or stress variation (Li et al., 2013) influences CBM production behavior (Clarkson and Qanbari, 2015). Thus, during drilling, production or injection of fluids during enhanced CBM production, and/or CO_2 sequestration there is a dynamic coal response. Unfortunately, volumetric data changes are not typically available due to the complexity of coal reservoirs (Liu and Harpalani, 2014), it can however be estimated by the matrix compressibility.

Mercury intrusion porosimetry (MIP) is widely used for determining the pore size distributionof porous materials and has applicability to conventional and unconventional reservoirs (e.g., tight sand, shales, and coals) (Labani et al., 2013; Lan et al., 2017; Liu et al., 2016; Song et al., 2018). However, during the experiment the coal matrix will be compressed and potentially damaged (Friesen and Mikula, 1988; Harpalani, 1999; Spitzer, 1981; Suuberg et al., 1995; Toda and Toyoda, 1972; van Krevelen, 1981). This volume reductions impacts the reservoir permeability and hense the CBM production (Meng et al., 2011). The apparent pore volume increase in MIP at >10 MPa is due to the coal compressibility (Toda and Toyoda, 1972; Cai et al., 2013; Guo et al., 2014). Multiple techniques have established that coal can have a range of pore sizes and a complex pore size distribution (Gan et al., 1972) composed of macropores (>50 nm), mesopores (2-50 nm) and micropores (<2 nm) by IUPAC (1982). There is a rank (and maceral/lithotype) influence on this pore size distribution and hence there is an expectation that the compress extent is rank dependent.

Coal matrix deformation can be divided into elastic deformation related to mechanical

decompression of the solid matrix, and non-elastic swelling induced by adsorption (Liu and Harpalani, 2014). As mercury is non-absorbing the non-elastic swelling can be neglected. Both experimental and theoretical methods have been developed to understand the compressibility of coals (Liu et al., 2015). As the applied mercury pressure increases, synchronous pore filling and compression may occur. Thus, determining the matrix compressibility of coals ranks capturing the effects of coal compressibility across the pressure range should be examined. Here, we suggest a theoretical approach to evaluate the compressibility of a coal rank range and establish the interrelationships between coal composition, moistures, ash yields, and pore structure to coal matrix compressibility. The distinguishing features of this work include 1) the evaluation of compressibility for different rank coals, 2) pore structure assessment using MIP and the N_2 adsorption isotherm at 77 K, and 3) factors affecting the coal matrix compressibility for different rank coals.

2. Methods

2.1. Coal sampling, and analyses

Here 39 coal blocks (30×30×30 cm^3), were selected from seven coal basins capturing: 7 low-rank (LRC, 0.49-0.65% $R_{o,m}$), 27 medium-rank (MRC, 0.66-1.90% $R_{o,m}$) and 5 high-rank coals (HRC, 2.00-2.95% $R_{o,m}$). Maximum vitrinite reflectance ($R_{o,m}$) (immersion in oil) and maceral composition were conducted with a microscope photometer (MPV-III, Leitz Company of Germany) following the GB/T 6948-1998 at China University of Geosciences at Beijing (CUGB). The $R_{o,m}$ varies from 0.49 to 2.95%, as listed in Table 1. Coal macerals were determined by the point counting technique following the scheme of the International Committee of Coal Petrology (ICCP, 1998). The coal composition varied, with vitrinite being 11.0-92.0%, inertinite of 0.6-78.8%

and a small amount of exinite of 0-18.2%, as well as some minerals (0-19.3%). Ash yields and inherent moisture contents were 2.45-28.28 wt% and 1.48-12.10 wt%. Proximate analysis was performed following the ASTM D7582-15 procedures (Pillalamarry et al., 2011). Helium porosimetry was determined using the routine core analysis methods as previous research (Cai et al., 2011). The helium porosity varies from 1.30% to 18.40%, as listed in Table 1. Cylindrical cores with diameters of 25 mm and lengths of 50 mm were acquired along the bedding face from coal blocks. These cores were used in the MIP experiment with the remaining coal being crushed to 60-80 mesh for N_2 adsorption/desorption analysis.

2.2. Mercury intrusion porosimetry and nitrogen adsorption/desorption

The MIP data was obtained using an Autopore 9420 Instrument (Micrometrics, US) using the coal cores. In using this approach to obtain the pore body radius with the aid of the Kelvin equation (Kelvin, 1871), it is necessary to assume: i) a model for the pore shape and ii) that the curvature of the meniscus is directly related to the pore width. The pore shape is generally assumed to be either cylindrical or slit-shaped (IUPAC, 1982). Here, the coal pore shape is assumed to be cylindrical. In the cylindrical case, the meniscus is hemispherical. The MIP analysis was conducted at the Coal Reservoir Laboratory of National Engineering Research Center of CBM Development & Utilization, China University of Geosciences at Beijing (CUGB), following the SY/T 5346-2005 standard procedure. Volume injection curves were obtained for each sample at pressure intervals of 0.0074-35 MPa, which corresponds to a pore-radius range of approximately 100 to 19 nm. Previous work (Busch et al., 2004; Han et al., 2013; Siemons et al., 2003 and Zhang, 2016) determined the sample size has no significant effect on the pore structure evaluation for the coal pore size <100nm. Coal pore structure will slightly differ between size fractions however. For instances, the pore volume ranges from ~0.01 to 0.3cm^3/g at different pore size when the particle

size is in the range of 10-3.35mm, 3.35-0.841mm, 0.841-0.25mm, 0.25-0.097mm and less than 0.097mm. However, there is no clear effect of coal particle size on the pore structure that from MIP experiment when the pore size less than 100nm (Zhang, 2016). The MIP curves were obtained as shown in Fig. 1. Before MIP analysis, all samples were dried at 75°C for 48 h. The low-temperature N_2 adsorption/desorption experiment was conducted using a Micromeritics ASAP-2000 with an equilibrium time of 6 min, respectively. The N_2 adsorption/desorption curves were acquired as presented in Fig. 2. The pore volume acquired from N_2 adsorption for all samples at the intervals of 0-100 nm range from 4.97×10^{-4} to 3.29×10^{-2} cm^3/g. The pore volumes for micropores (<2 nm), mesopores (2-50 nm) and macropores (>50 nm) are shown in Fig. 3. For the pore volume acquired using N_2 adsorption, there is slight pore volume variation (~0.1×10^{-3} -1.1×10^{-3} cm^3/g) when coal particle sizes range from 10-3.35mm, 3.35-0.841mm, 0.841-0.25mm, 0.25-0.097mm to less than 0.097mm (Zhang, 2016). Here, the 60-80 mesh cut (~0.25-0.18mm) was used. This particle size has no obvious effect on pore structure evaluation by N_2 for the coals with pore size less than 100 nm (Zhang, 2016). Therefore, the pores with size of 19-100 nm were selected to investigate the matrix compressibility of different rank coals by mercury intrusion porosimetry and N_2 adsorption. Experimental and data processing procedures are the same as presented in our previous work (Cai et al., 2013; Cai et al., 2017).

2.3. Coal Matrix Compressibility

Mercury is nonwetting on sedimentary materials including sandstone, carbonates, shale, and coals. Mercury overcomes capillary resistance to enter the pores when the mercury pressure is greater than or equal to the capillary pressure at the pore throat. Here, the typical assumption is the cylindrical pore shape. Assuming the pores are composed of a variety of cylindrical pores, the Washburn equation (Washburn, 1921) can be used to obtain the pore radius, as shown in Equation

(1):

$$P_c = -\frac{2\sigma \cos\theta}{r_c} \quad (1)$$

where P_c is the pressure (MPa); σ is the surface tension (N/m), set to be 0.48 N/m; θ is the wetting contact angle (°), set to be 135°; and r_c is the capillary radius (μm) at the corresponding pressure. Therefore, after substituting:

$$P_c = \frac{0.679}{r_c} \quad (2)$$

According to Equation (2), the pore radius can be obtained from MIP data.

Coal matrix compressibility, if neglecting mercury compressibility, can be defined as (Li et al., 1999):

$$C_m = \frac{dV_m}{V_m dP} \quad (3)$$

where dV_m / dP is the volume change of coal matrix as a function of pressure and V_m is the coal matrix volume. The V_m is calculated as:

$$V_m = \frac{1}{\rho} - V_T \quad (4)$$

where ρ is the density of coal samples (g/cm^3) and represents the reciprocal of the total volume of the coal sample; V_T (cm^3/g) is BJH (Barrett et al., 1951) pore volume, which represents total pore volume of coal samples. The BJH theoretical model was based on the BET multilayer adsorption theory and capillary condensation of vapors in the porous material (Barrett et al., 1951). The N_2 adsorption isotherms were measured for relative pressures ranging from 0.01 to 0.99 to obtain pore BET surface area, BJH pore volumes and the pore size distributions.

Significant compression in coals can be detected with increasing mercury intrusion. For a

compressible porous solid, the relationship is:

$$\Delta V_{mercury} = \Delta V_{pore} + \Delta V_{compaction} \quad (5)$$

where $\Delta V_{mercury}$ represents the observed increase in mercury volume that comes from pore filling ΔV_{pore} and solid compression $\Delta V_{compaction}$, respectively.

In this experiment, the pressure is set at 6.80-35.03 MPa, which corresponds to the pressure interval of 100 nm-19 nm (Equation 2). Thus, at 6.80-35.03 MPa pressure, the fractures/cleats (>100 nm) space have been filled with non-compressible mercury, and thus, it can be assumed to be unchangeable with the increasing mercury intrusion pressure during the MIP measurements. Meanwhile, the observed mercury volume change is equal to the sum of the coal matrix compression volume and the filling volume of the pore size of 19−100 nm. From relationship between mercury volumes and pressures, $\Delta V_{mercury} / \Delta P$ can be assumed to be a constant, N. Therefore, we can approximate using (Cai et al., 2013; Guo et al., 2014; Li et al., 1999):

$$\frac{\Delta V_{compaction}}{\Delta P} = \mathrm{N} - \frac{\sum_{19nm}^{100nm} \Delta V_{pore}}{\Delta P} \quad (6)$$

Previous research (Mahajan, 1991) has shown that N_2 sorption may severely underestimate pore numbers (especially small pores) in high-rank. Therefore, here the pore volumes (PV) with pore sizes of 19-100 nm are estimated from N_2 adsorption/desorption data to avoid this. Constant $\Delta V_{mercury} / \Delta P$ or $\Delta V_{compaction} / \Delta P$ is valid only if the pores included in the sample remain unchanged during compression. Assuming $\Delta V_{compaction} / \Delta P$ is independent of pressure, and replacing dV_m / dP by $\Delta V_{compaction} / \Delta P$. Combined with Equations (3) and (6), the coal matrix compressibility can be acquired:

$$C_m = \frac{1}{V_m}\left(\mathrm{N} - \frac{\sum_{19nm}^{100nm} \Delta V_{pore}}{\Delta P}\right) \quad (7)$$

where the coal matrix compressibility has an average of 6.80-35.03 MPa.

3. Results

3.1. Coal characteristics

The 39 coal samples were divided into three coal ranks: low-rank coals ($R_{o,\ m}$<0.65%), medium-rank coals (0.65%<$R_{o,\ m}$<1.9%) and high-rank coals ($R_{o,\ m}$>1.9%). These coals vary markedly in their maceral and minerals contents, which represent a wide range in composition, as shown in Table 1. The volume contents for vitrinite, inertinite and exinite are in the range of 11-92.04%, 0.6-78.08% and 0-18.2%, respectively. Exinite disappears when the maximum vitrinite reflectance is over 1.19%. The mineral volume content varies from 0 to 19.3%. These variable macerals and mineral contents will impact gas adsorption and the pore filling minerals, (from paleo-fluid flow and mineralization) occlude some pores (Crosdale et al., 1998). Ash yields of these coals vary from 2.45-28.28% and moisture contents vary from 0.2-12.1%. Moistures in matrix pores have a great impact on not only gas diffusion and flow but also on coal matrix compressibility (Pan et al., 2010). The petrophysical analysis shows that the porosities of these coals change greatly (1.3-20.8%) as listed in Table 1. These results are comparable to the coals of the same ranks based on previous research (Cai et al., 2016).

3.2. Pore structures from MIP and N_2 adsorption/desorption at 77 K

Based on the MIP curves, different types of pore structures are revealed as shown in Fig. 1. Previous research has revealed that coals with high inertinite and high ash yields have greater mesoporosity and less microporosity than coals of the same rank with high vitrinite and low ash yields (Crosdale et al., 1998; Cai et al., 2013). For LRC samples, the maximum intruded mercury volume ranges from 0.005~0.13 cm^3/g, and the ascending curve normally goes steadily upward, as shown in Fig. 1. The steadily rising curve may be due to the three peaks of pores in low-rank coals

as revealed by our previous research (Cai et al., 2016). For medium-rank coals and high-rank coals, the maximum intruded mercury volume are generally lower than 0.09 cm^3/g, and the ascending curve normally goes up sharply. This phenomenon is likely related to the large amount of micropores in the medium and high-rank coals.

Fig. 2 shows the N_2 adsorption/desorption curves at 77 K for typical coals of different ranks. The Type II reversible isotherms are for all selected samples LRC1, LRC4, MRC8 MRC18, HRC1 and HRC4 according to the IUPAC classifications (IUPAC, 1982), which represents unrestricted monolayer-multilayer adsorption. The beginning of the nearly linear middle section of the isotherm is often taken to indicate the stage at which monolayer coverage is complete and multilayer adsorption is about to begin. Hysteresis loops also occur for all selected samples, which normally indicate that hysteresis that appears in the multilayer range of physiosorption isotherms is usually associated with capillary condensation in mesopores, especially for the priority for mesopore volumes (e.g., LRC4, MRC8 and HRC4 in Fig. 3). Hysteresis loops can exhibit variable pore shapes. The hysteresis loops that terminate (desorption branch) at a relative pressure of 0.42 (nitrogen at its boiling point at p/p° 0.42) indicate slit-like/plate-like pores (for MRC18, HRC1 and HRC4) and ink-bottle pores (for MRC8), which correspond to type H3 loop and approximate type H2 loop, respectively (Sing et al., 1985). The type H3 loop is deemed as an aggregate of plate-like particles that give rise to slit-shaped pores. The H2 loop may be attributed to the difference in N_2 condensation and evaporation processes that occur in pores with narrow necks and wide bodies (often referred to as ink-bottle pores) and the role of network effects. The LRC1 and LRC4 belong to the Type H4 loop that is often associated with narrow slit-like pores.

3.3. Calculated coal matrix compressibility

Based on the MIP and N_2 adsorption/desorption data, the coal matrix compressibility of all 39 coal

samples with pore sizes of approximately 19-100 nm were calculated as shown in Table 2. There is a clear linear relationship between the mercury volume and pressure for all samples within the pressure interval of 6.80-35.03 MPa. Therefore, the values of the constant N that results from the slopes of the fitted linear relationships are obtained as presented in Table 2. Then, on the basis of Equation 7, the coal matrix compressibility for all samples can be acquired. Before system evaluation of coal matrix compressibility, the estimate of the error introduced by experiments, and the compressibility value errors at 30 MPa would be lower than 4% and can probably be ignored for most purposes. The computed coal matrix compressibility varies greatly with values of 0.24-13.56×10^{-4} MPa^{-1}. The coal matrix compressibility values of the LRC, MRC, and HRC coals are 1.44-13.26×10^{-4} MPa^{-1} with an average of 6.93×10^{-4} MPa^{-1}, 0.24-13.56×10^{-4} MPa^{-1} with an average of 3.12×10^{-4} MPa^{-1} and 0.25-0.91×10^{-4} MPa^{-1} with an average of 0.25×10^{-4} MPa^{-1}.

4. Discussion

4.1. Effects of coal rank on coal matrix compressibility

Coal matrix compressibility shows a negative exponential relationship as coal rank increases, as shown in Fig. 4(a). The coal matrix compressibility values of low-rank coals emerge as a rapid decrease from 13.26×10^{-4} MPa^{-1} to 1.44×10^{-4} MPa^{-1} as coal rank increases from 0.49% to 0.65% $R_{o,m}$ as listed in Table 2. The average coal matrix compressibility for low-rank coals is 6.93×10^{-4} MPa^{-1}. For medium-rank coals (0.65%-1.9% $R_{o,m}$), the coal matrix compressibility decreases slowly from 13.56×10^{-4} MPa^{-1} to 0.24×10^{-4} MPa^{-1} as coal rank increases. The average coal matrix compressibility for medium-rank coals is 3.12×10^{-4} MPa^{-1}. For high-rank coals, the coal matrix compressibility declines slightly from 0.91×10^{-4} MPa^{-1} to 0.25×10^{-4} MPa^{-1} as coal rank increases 2.0%-2.95% $R_{o,m}$. Guo et al. (2014) examined the coals with rank of $R_{o,max}$=0.65–0.88%, the

matrix compressibility ranges from 2.01 to 2.74×10^{-4} MPa^{-1}; Li et al. (1999) presented a subbituminous coal and a bituminous coal with the matrix compressibility of $2.50\text{-}3.13\times10^{-4}$ MPa^{-1}; Toda and Toyoda (1972) and Spitzer (1981) examined the coals with carbon of 72.7–93.2%, the matrix compressibility were in the range of $0.7\text{-}2.3\times10^{-4}$ to $1.72\text{-}2.09\times10^{-4}$ MPa^{-1} respectively. And Cai et al. (2013) shows the coal matrix compressibility varies from 1.55×10^{-4} MPa^{-1} to 2.37×10^{-4} MPa^{-1} with the $R_{o,max}$=0.54-1.19%. Recently, Song et al. (2018) reveals that the coal matrix compressibility of coals with $R_{o,max}$=0.63-0.81% are in the range of $3.24\text{-}4.24\times10^{-4}$ MPa^{-1}. Using the above calculation method, the coal matrix compressibility for selected coals ($0.24\text{-}13.56\times10^{-4}$ MPa^{-1}) obviously present a wider range than the values calculated by previous research (Cai et al., 2013; Guo et al., 2014; Li et al., 1999; Song et al., 2018; Spitzer, 1981; Toda and Toyoda, 1972) due to the wide and consecutive coal rank with $R_{o,max}$ of 0.49–2.95%.

Table 3 shows the difference in pore volume (19-100 nm) between the MIP and N_2 adsorption methods. The results show that a big difference exists and a decreasing trend between the differences of pore volume and coal rank. The effect of coal rank on coal matrix compressibility is probably due to significant chemical and physical changes that occur in the coals. For low-rank coals, the basic unit of the macromolecular structure of coal is randomly distributed and forms an open structure under the joint and support of numerous oxygen-containing functional groups and aliphatic side chains (Yu et al., 2013; Vega et al., 2017). With mechanical compaction, dehydration and degassing during coalification, the volume of the coal matrix changes greatly. Therefore, the coal matrix compressibility decreases rapidly in low coal rank coals. After the subbituminous stage of coalification, the lengths of the organic side chains of the coal become shorter and their

number decreases (He et al., 2017). Meanwhile, the condensed nucleus of humus complex increases, and then follows the increase in molecular weight, the slow increase in condensed aromatic rings and the gradual regularization of the molecular arrangement (Mayumi et al., 2016). Therefore, the coal matrix compressibility of the medium and high-rank coals emerges as a slow decreasing trend with increasing rank.

4.2. Effects of macerals and minerals on coal matrix compressibility

Macerals of the investigated coals are mainly composed of vitrinite, inertinite and exinite. A portion of the investigated coals lack exinites due to thorough metamorphism when the vitrinite reflectance reaches 1.19% $R_{o,m}$ as listed in Table 1. Coal matrix compressibility correlates well with the vitrinite and inertinite, especially for low-rank coals. However, the exinite content has a fine relationship with the coal matrix compressibility of medium-rank coals, as shown in Fig. 5. For low and high-rank coals, the vitrinite and inertinite have significant effects on the coal matrix compressibility, which should be related to the brittle features and multiple micropores in vitrinite (Liu et al., 2017; Keshavarz et al., 2017), and stiffness features, mesopores, macropores and pyrites and clay minerals filled with the inertinite as shown in Fig. 6, especially for high-rank coals. An abundance of micropores in vitrinite causes the matrix to be difficult to compress. For the medium-rank coals, the coal matrix compressibility seems independent of the maceral composition except slight relation with exinite, which is possibly due to the limited samples of medium coal rank coals.

Interestingly, for high-rank coals, the vitrinite and inertinite have a complex relationship with the coal matrix compressibility, as shown in Fig. 5. There is an opposite relationship between inertinite and coal matrix compressibility for low and high-rank coals. The inertinite normally

contains a large amount of meso- and macropores, as revealed by previous research (Giffin et al., 2013). The reason for this opposite phenomenon is the meso- and macropores and minerals in the inertinite. For low-rank coals, the meso- and macropores have greater impacts on matrix compressibility than the minerals have on matrix compressibility. Therefore, the compressibility increases with increasing inertinite content. In contrast, the inertinite situation for high-rank coals is the opposite, which is due to the minerals that are filled with meso- and macropores during deep coal metamorphism (Li et al., 2017). The mineral content in volume ranges from 0-19.3%, as listed in Table 1. Although there is generally a negative exponential relationship between mineral content and coal matrix compressibility, as shown in Fig. 4(b), the data points vary. Although most minerals that occur in coal matrix pores could strengthen the matrix compressibility (Tao et al., 2018), the existence of minerals, including those filling pores or not, also have an impact on coal matrix compressibility. For a few types of minerals, such as clay minerals, these minerals may not reinforce the matrix compressibility because of the pores that exist in these minerals.

4.3. Effects of moisture and ash yields on coal matrix compressibility

Fig. 7 shows that coal matrix compressibility increases linearly with increasing moisture content for all samples (correlation coefficient is 0.49). For low-rank coals, the coal matrix compressibility increases exponentially with increasing moisture content with correlation coefficient of 0.81. This result indicates that the moisture softening of coal could be significant. The wetting action of water molecules weakens the link between coal particles, which will weaken the mechanical properties of coals (Yu et al., 2013; Wu et al., 2017). Meanwhile, the water in the pores and fractures will produce pressure (Su et al., 2017), which will also reduce the elastic modulus of coals and improve the deformation ability, leading to easy compression deformation of the coal

matrix. Therefore, the moistures in low-rank coals can significantly increase the coal matrix compressibility response. Another reason that the moisture in low-rank coals raises the coal matrix compressibility is the more open structure of the low-rank coals that have not experience high pressure compaction during of coalification. The loss of moisture can lead to consolidation of the coal structure and shrinkage (Suuberg et al., 1993), which will reduce the coal matrix compressibility. Pan et al. (2010) illustrated that moisture in the coal matrix would cause coal shrinkage and changes in mechanical properties, thereby impacting coal permeability in reservoir conditions.

Therefore, relatively high moistures can result in high coal matrix compressibility for low-rank coals. For medium-rank coals, the moisture content has a subtle linear relationship with coal matrix compressibility due to further compaction of the coal matrix after the early stage of coalification. For high-rank coals, as shown in Fig. 7(d), there is a subtle relationship between moisture and coal matrix compressibility. The coal matrix compressibility values have a decreasing trend with increasing moisture content from 0.62 to 1.03%. After that, the coal matrix compressibility follows an increasing trend with increasing moisture content. This phenomenon may originate from the limited available data for high-rank coals.

Fig. 8(a) shows that porosity generally decreases with increasing ash yields for different rank coals even though the correlation coefficient varies, indicating that minerals fill the pores through mineralization and decrease the porosity of the coal. Fig. 8(b) shows that the relationship between coal matrix compressibility and ash yields demonstrating the matrix is not easily compressed for coals with high mineral matter content.

4.4. Effects of pore structure on coal matrix compressibility

Fig. 9(a) shows a generally positive relationship between coal matrix compressibility and porosity. As coal rank increases, the effect of porosity on coal matrix compressibility decreases (low coal rank R^2=0.92; medium coal rank R^2=0.46; high coal rank R^2=0.30). For low coal rank coals, the matrix compressibility quickly increases as porosity increases, which means that the porosity is a critical parameter that affects matrix compressibility for low-rank coals. As shown in Fig. 9(b). The porosity of medium-rank coals and the associated matrix compressibility shows a similar U-shaped curve, which decreases slightly as porosity increases from 0.00-4.13%, and then increases as porosity exceeds 4.13%. The relationship between the porosity of high-rank coals and matrix compressibility is analogous to that of medium-rank coals, as shown in Fig. 9(c) and 9(d).

As shown in Fig. 10, there is an inverted, slight U-shaped relationship between total pore volume and coal matrix compressibility. As coal rank increases, the influence of total pore volume on coal matrix compressibility is also larger (low coal rank R^2< 0.1; medium coal rank R^2= 0.48; high coal rank R^2= 0.87). An interesting phenomenon is observed here. For low-rank coal, the total pore volume has no significant effect on coal matrix compressibility, whereas the porosity has a significant influence. For medium-rank coals, the total pore volume and porosity both affect coal matrix compressibility. For high-rank coals, the influence of total pore volume on coal matrix compressibility is greater than that of porosity. This phenomenon indicates that porosity and total pore volume are coordinated factors that affect matrix compressibility. For low-rank coals, the pores are composed of a large amount of mesopores and macropores, as shown in Fig. 3. Therefore, the greater the porosity indicates the lower the matrix compressibility. However, the condition for high-rank coals is the opposite of low-rank coals. There are abundant micropores that have diameters less than 100 nm, accounting for over 75% of the porosity as revealed by

previous research (Cai et al., 2011). These micropores will resist the matrix compressibility. The influences of coal rank on the coal matrix compressibility should also be attributed to the micropore pore volumes as previous research confirmed (Guo et al., 2014; Song et al., 2018). Smaller mesopores and micropores gradually play dominant roles (Nie et al., 2015; Pan et al., 2016). Therefore, the total pore volume is more important for matrix compressibility than porosity. By observing the effects of different pore sizes on matrix compressibility (Fig. 11), we found that mesopores are dominant within the different pores group, normally over 60% for medium and high-rank coals and over 85% for the low-rank coals for pores less 100 nm. The micropores and macropores account for less than 30% for different rank coals. The microporosity, mesoporosity and macroporosity have diverse impacts on coal matrix compressibility. For low and medium-rank coals, macropores have significant positive impacts on matrix compressibility compared to mesopores and micropores, as shown in Fig. 11(a) and (b). However, for high-rank coals, the mesopores have significant positive impacts on matrix compressibility compared to macropores and micropores, as shown in Fig. 11(c). These results indicate that the mesopores and macropores are critical for matrix compressibility, whereas micropores can effectively resist coal matrix compressibility.

5. Conclusions

Mercury intrusion porosimetry can be used as an effective means to evaluate pore structure, provided the matrix compressibility of coals associated with this method can be evaluated through N_2 adsorption/desorption at 77 K. Factors that affect coal matrix compressibility were discussed herein. We determined that the coal matrix compressibility varies from 0.24×10^{-4} MPa^{-1} to 13.56×10^{-4} MPa^{-1} as coal rank changes. The following conclusions are made:

1) Coal matrix compressibility follows an exponential decreasing trend with increasing coal rank. The coal matrix compressibility decreases rapidly in low-rank coals due to mechanical compaction, dehydration and degassing during coalification. The coal matrix compressibility of medium and high-rank coals shows a slow decreasing trend with increasing rank.

2) There is an opposite relationship between inertinite and coal matrix compressibility for low and high-rank coals due to the meso- and macropores and minerals in the inertinites. For low-rank coals, the meso- and macropores have greater impacts on matrix compressibility than the minerals have on matrix compressibility. In contrast, the inertinite situation for the high-rank coal is the opposite, which is because the minerals are filled in meso- and macropores.

3) For low-rank coals, the moisture in coals may have a significant effect on the coal matrix compressibility because the wetting action of water molecules weakens the link between coal particles, reduces the elastic modulus of coals and improves the deformation capacity.

4) The mineral appearance, including whether minerals fill pores or not, also has an impact on coal matrix compressibility. There is a generally a negative exponential relationship between mineral content and coal matrix compressibility. For a few types of minerals, such as clay minerals, the minerals may not reinforce the matrix compressibility due to the pores that exist in the minerals.

5) Micro-, meso- and macroporosity have diverse impacts on coal matrix compressibility. The mesoporosity and macroporosity in coals are critical for effective changes in coal matrix compressibility, whereas the micropores are less effected.

Acknowledgements

This research was funded by the National Natural Science Fund (grant nos. 41830427, 41602170 and 41772160), the National Major Research Program for Science and Technology of China (grant no. 2016ZX05043-001), the Key Research and Development Projects of the Xinjiang Uygur Autonomous Region (grant no. 2017B03019-01) and the Research Program for Excellent Doctoral Dissertation Supervisor of Beijing (grant no. YB20101141501).

Nomenclature

P_c , The pressure at which mercury enters pores (MPa)

σ , The surface tension (N/m)

θ, The wetting contact angle (°)

r_c , The capillary radius at the corresponding pressure (μm)

C_m , Coal matrix compressibility (MPa^{-1})

V_m , The coal matrix volume (cm^3/g)

dV_m / dP , The volume change of coal matrix as a function of pressure

$\Delta V_{mercury}$, The observed increase in mercury volume (cm^3/g)

ΔV_{pore} , Pore filling volume (cm^3/g)

$\Delta V_{compaction}$, Solid compression volume (cm^3/g)

References

Barrett, E.P., Joyner, L.G., Halenda, P.P., 1951. The determination of pore volume and area distributions in porous substances. 1. Computations from nitrogen isotherms. J. Am. Chem. Soc. 73 (1), 373–380.

Busch, A., Gensterblum, Y., Krooss, B.M., Littke, R., 2004. Methane and carbon dioxide adsorption–diffusion experiments on coal: upscaling and modeling. Int J Coal Geol 60,151–68.

Cai, Y., Liu, D., Liu, Z., Zhou, Y., Che, Y., 2017. Evolution of pore structure, submaceral composition and produced gases of two Chinese coals during thermal treatment. Fuel Process. Technol. 156, 298-309.

Cai, Y., Liu, D., Pan, Z., Che, Y., Liu, Z., 2016. Investigating the effects of seepage-pores and fractures on coal permeability by fractal analysis. Transport Porous Med. 111, 479-497.

Cai, Y., Liu, D., Pan, Z., Yao, Y., Li, J., Qiu, Y., 2013. Pore structure and its impact on CH_4 adsorption capacity and flow capability of bituminous and subbituminous coals from Northeast China. Fuel 103, 258-268.

Cai, Y., Liu, D., Yao, Y., Li, J., Qiu, Y., 2011. Geological controls on prediction of coalbed methane of No. 3 coal seam in Southern Qinshui Basin, North China. Int. J. Coal Geol. 88, 101-112.

Clarkson, C.R., Qanbari, F., 2015. Transient flow analysis and partial water relative permeability curve derivation for low permeability undersaturated coalbed methane wells. Int. J. Coal Geol. 152,110-124.

Crosdale, P.J., Beamish, B.B., Valix, M., 1998. Coalbed methane sorption related to coal

composition. Int. J. Coal Geol. 35, 147-158.

Friesen, W.I., Mikula, R.J., 1988. Mercury porosimetry of coals - pore volume distribution and compressibility. Fuel, 67, 1516-1520

Gan, H., Nandi, S.P., Walker,P.L., 1972. Nature of the porosity in American Coals. Fuel, 51, 272-277.

Giffin, S., Littke, R., Klaver, J., Urai, J.L., 2013. Application of BIB-SEM technology to characterize macropore morphology in coal. Int. J. Coal Geol. 114, 85-95.

Guo, X., Yao, Y., Liu D., 2014. Characteristics of coal matrix compressibility: an investigation by mercury intrusion porosimetry. Energy Fuel. 28, 3673−3678.

Han, F., Busch, A., Krooss, B.M., Liu, Z., Yang, J., 2013. CH_4 and CO_2 sorption isotherms and kinetics for different size fractions of two coals. Fuel 108, 137−142.

Harpalani, S., 1999. Compressibility of coal and its impact on gas production from coalbed reservoirs. In: Vail Rocks 1999 The 37th US Rock Mechanics Symposium (USRMS), Vail, Colorado, USA. Rock Mechanics for Industry, Amadei B, Kranz RL, Scott GA, Smeallie PH(Eds.), American Rock Mechanics Association pp. 301–308

He, X., Liu, X., Nie, B., Song, D., 2017. FTIR and Raman spectroscopy characterization of functional groups in various rank coals. Fuel 206, 555-563.

ICCP., 1998. The new vitrinite classification (ICCP System 1994). Fuel 77, 349-358.

IUPAC., 1982. Reporting physisorption data for gas/solid systems with special reference to the determination of surface area and porosity. Pure Appl. Chem. 54, 2201-2218.

Keshavarz, A., Sakurovs, R., Grigore, M., Sayyafzadeh, M., 2017. Effect of maceral composition and coal rank on gas diffusion in Australian coals. Int. J. Coal Geol. 173, 65-75.

Labani, M.M., Rezaee, R., Saeedi, A., Al Hinai, A., 2013. Evaluation of pore size spectrum of gas shale reservoirs using low pressure nitrogen adsorption, gas expansion and mercury porosimetry: A case study from the Perth and Canning Basins, Western Australia. J. Petro. Sci. Eng. 112, 7-16.

Lan, Y., Davudov, D., Moghanloo, R.G., 2017. Interplay between permeability and compressibility in shale samples. J. Petro. Sci. Eng. 159, 644-653.

Li, S., Tang, D., Pan, Z., Xu, H., Huang, W., 2013. Characterization of the stress sensitivity of pores for different rank coals by nuclear magnetic resonance. Fuel 111, 746−754.

Li, Y., Lu, G., Rudolph, V., 1999. Compressibility and fractal dimension of fine coal particles in relation to pore structure characterisation using mercury porosimetry. Part Part. Syst. Charact. 16, 25–31.

Li, Z., Liu, D., Cai, Y., Ranjith, P.G., Yao, Y., 2017. Multi-scale quantitative characterization of 3-D pore-fracture networks in bituminous and anthracite coals using FIB-SEM tomography and X-ray mu-CT. Fuel 209, 43-53.

Liu, P., Yuan, Z., Li, K., 2016. An improved capillary pressure model using fractal geometry for coal rock. J. Petro. Sci. Eng. 145, 473-481.

Liu, S., Harpalani, S., 2014. Compressibility of sorptive porous media: Part 1. Background and theory. AAPG Bulletin 98, 1761–1772.

Liu, Y., Zhu, Y., Li, W., Zhang, C., Wang, Y., 2017. Ultra micropores in macromolecular structure of subbituminous coal vitrinite. Fuel 210, 298-306.

Liu, Z., Guan, D., Wei, W., Davis, S.J., Ciais, P., Bai, J., et al., 2015. Reduced carbon emission estimates from fossil fuel combustion and cement production in China. Nature 524, 335-338.

Mahajan, O.P., 1991. CO_2 surface area of coals - the 25-year paradox. Carbon 29, 735-742.

Mayumi, D., Mochimaru, H., Tamaki, H., Yamamoto, K., Yoshioka, H., Suzuki, Y., et al., 2016. Methane production from coal by a single methanogen. Science 354, 222-225.

Meng, Z.P., Zhang, J. C., Wang, R., 2011. In-situ stress, pore pressure and stress-dependent permeability in the southern Qinshui Basin. Int. J. Rock Mech. Min. Sci. 48, 122-131.

Nie, B., Liu, X., Yang, L., Meng, J., Li, X., 2015. Pore structure characterization of different rank coals using gas adsorption and scanning electron microscopy. Fuel 158, 908-917.

Palmer, I., Mansoori, J.,1998. How permeability depends on stress and pore pressure in coalbeds: a new model. SPEREE 1 (6), 539-544.

Pan, J., Wang, K., Hou, Q., Niu, Q., Wang, H., Ji, Z., 2016. Micro-pores and fractures of coals analysed by field emission scanning electron microscopy and fractal theory. Fuel 164, 277-285.

Pan, Z., Connell, L.D., Camilleri, M., Connelly, L., 2010. Effects of matrix moisture on gas diffusion and flow in coal. Fuel 89, 3207-3217.

Pillalamarry, M., Harpalani, S., Liu, S., 2011. Gas diffusion behavior of coal and its impact on production from coalbed methane reservoirs. Int. J. Coal Geol. 86, 342-348.

Siemons, N., Busch, A., Bruining, H., Krooss, B.M., Gensterblum, Y., 2003. Assessing the kinetics and capacity of gas adsorption in coals by a combined adsorption/diffusion method. SPE 84340. Annual Technical Conference and Exhibition, 5 – 8 October, Denver.

Sing, K.S.W., Everett, D.H., Haul, R.A.W., Moscou, L., Pierotti, R.A., Rouquerol, J., et al., 1985. Reporting physisorption data for gas/solid systems with special reference to the determination of surface area and porosity. Pure Appl. Chem. 57, 603-619.

Song, Y., Jiang, B., Shao, P., Wu, J., 2018. Matrix compression and multifractal characterization for tectonically deformed coals by Hg porosimetry. Fuel 211, 661-675.

Spitzer, Z., 1981. Mercury porosimetry and its application to the analysis of coal pore structure. Powder Techno. 29, 177-186.

Su, X., Wang, Q., Song, J., Chen, P., Yao, S., Hong, J., et al., 2017. Experimental study of water blocking damage on coal. J. Petro. Sci. Eng. 156, 654-661.

Suuberg, E. M., Otake, Y. Y., Deevi, S. C., 1993. Role of moisture in coal structure and the effects of drying upon the accessibility of coal structure. Energy Fuel. 7,384−392.

Suuberg, E.M., Deevi, S.C., Yun, Y.S., 1995. Elastic behavior of coals studied by mercury porosimetry. Fuel, 74, 1522-1530

Tao, S., Chen, S., Tang, D., Zhao, X., Xu, H., Li, S., 2018. Material composition, pore structure and adsorption capacity of low-rank coals around the first coalification jump: A case of eastern Junggar Basin, China. Fuel 211, 804-815.

Thomson, W. T., (Lord Kelvin). On the equilibrium of vapour at a curved surface of liquid. Philos . Mag. 1871, 42: 448-452.

Toda, Y., Toyoda , S., 1972. Application of mercury porosimetry to coal. Fuel, 51, 199-201.

van Krevelen, D.W., 1981. Coal Typology Chemistry Physics Constitution, 2nd ed. Elsevier, Amsterdam.

Vega, M.F., Acevedo, B., Diaz-Faes, E., Barriocanal C., 2017. Effect of mild oxidation on the surface chemistry of bituminous coals under different humidity conditions. Int. J. Coal Geol. 179, 164-172.

Washburn, E.W., 1921. The dynamics of capillary flow. Phys. Rev. 17, 273-283.

Wu, J., Wang, J., Liu, J., Yang, Y., Cheng, J., Wang, Z., et al., 2017. Moisture removal mechanism of low-rank coal by hydrothermal dewatering: Physicochemical property analysis and DFT

calculation. Fuel 187, 242-249.

Yu, J., Tahmasebi, A., Han, Y., Yin, F., Li, X., 2013. A review on water in low-rank coals: The existence, interaction with coal structure and effects on coal utilization. Fuel Process. Technol. 106, 9-20.

Zhang, J., 2016. Experimental study and modeling for CO_2 diffusion in coals with different particle sizes: based on gas absorption (imbibition) and pore structure. Energy Fuels 30, 531−543.

Captions for Figures and Tables

Fig. 1. MIP curves of different coal ranks: (a) <0.65% $R_{o,m}$, (b) 0.65-2.0% $R_{o,m}$, and (c) >2.0% $R_{o,m}$.

Fig. 2. N_2 adsorption/desorption at low temperature (77K) of different rank coals. a (LRC1) and b (LRC4) belong to the Type H4 loop that often associated with narrow slit-like pores; c(MRC8) may indicate ink-bottle pores with type H2 loop; d(MRC18), e(HRC1) and f(HRC4) may indicate slit-like/plate-like pores with type H3 loop.

Fig. 3. Pore volume distribution of variable rank coals at different sizes. (a) displays the pore volume distribution of low-rank coals; (b) shows the variable pore volume distribution of medium-rank coals; (c) exhibits the pore volume distribution of high-rank coals.

Fig. 4. Relation between vitrinite reflectance ($R_{o,m}$), mineral contents of variable coals and coal matrix compressibility. (a) shows a negative exponential relation between $R_{o,m}$ and coal matrix compressibility; (b) displays a negative exponential relation between mineral contents and coal matrix compressibility.

Fig. 5. Relations between maceral composition and coal matrix compressibility. (a) shows a clear negative relation between vitrinite content and matrix compressibility for low-rank coals; (b) displays an obvious increase trend between inertinite and matrix compressibility for low-rank coals; (c) exhibits no clear relation between exinite content and for low-rank coals; No clear relations between vitrinite (d), inertinite (e), exinite (f) contents and matrix compressibility for medium-rank coals; (g) and (h) show no clear relation existed between vitrinite, inertinite and matrix compressibility in high-rank coals.

Fig. 6. Minerals in selected coals. a(MRC24): Telinite (T) is fragmented. Collinite (C) presented in bands and aggregates. Semivitrinite (SV) and Semifusinite (Sf) mostly appear in lenticular form and fractures fill with pyrite veins; b(MRC26): A large amount of pyrite pellets are dispersedly distributed in collinite (C). Semifusinite (Sf) is in ellipsoidal and lenticular. Pores filled with clay minerals (Cl) are clear; c(MRC27): Telinite (T) is distributed in a wide band. Pores are easily deformed and filled with clay minerals (Cl). Semifusinite (Sf) is granulated in

collinite. Pyrite (Py) is in a cluster distribution; d(HRC1): Collinite (C) is locally fragmented and filled with euhedral and semi-euhedral pyrite (Py), which shows metasomatism; e(HRC2): Collinite (C), telinite (T) and semivitrinite (SV) are distributed alternately, presenting in band or detritus. A few of semifusinite (SF) debris are sporadic. Clay minerals (Cl) exhibited in lump or filled in pores, and occasional pyrite (Py); f(HRC3): Telinite (T) and semitelinite (ST) with broken granular structure are closely associated. Pores are filled with clay minerals (Cl), occasionally particulate pyrite (Py).

Fig. 7. Relations between moisture content in coals and coal matrix compressibility. (a) shows a general linear relation between moistures from all rank coals and matrix comressbility; (b) exhibits a positive exponential relation between moistures content and matrix compressibility in LRCs; (c) displays a slight linear relation between moistures from MRCs and matrix comressbility; (d) displays no clear relation between moistures from HRCs and matrix comressbility.

Fig. 8. Relations between porosity, matrix compressibility and ash yields. (a) ash yields versus porosity and (b) ash yields versus coal matrix compressibility

Fig. 9. Relationship between porosity of the different rank coals and coal matrix compressibility. (a) coal matrix compressibility versus porosities from all rank coals present an exponential relation; (b) exhibits a positive relation between coal matrix compressibility and porosities from LRC; (c) shows a general exponential relation between matrix compressibility and porosities in MRCs; (d) presents an U shaped relation between matrix compressibility and porosities in HRCs.

Fig. 10. Relations between total pore volume of different rank coals and coal matrix compressibility. (a) shows a reversed U shaped relation with all samples; (b) no clear relation; (c) and (d) show reversed U shaped relation.

Fig. 11. Relationship between pore size ratio of the different coal ranks and coal matrix compressibility. (a) low-rank coals; (b) medium-rank coals; (c)high-rank coals

Table 1 Sample information and basic parameters of the selected Chinese coals

Table 2 Calculation parameters of the coal matrix compressibility for different rank coals

Table 3 The difference of pore volume (19-100nm) between MIP and N_2 adsorption methods

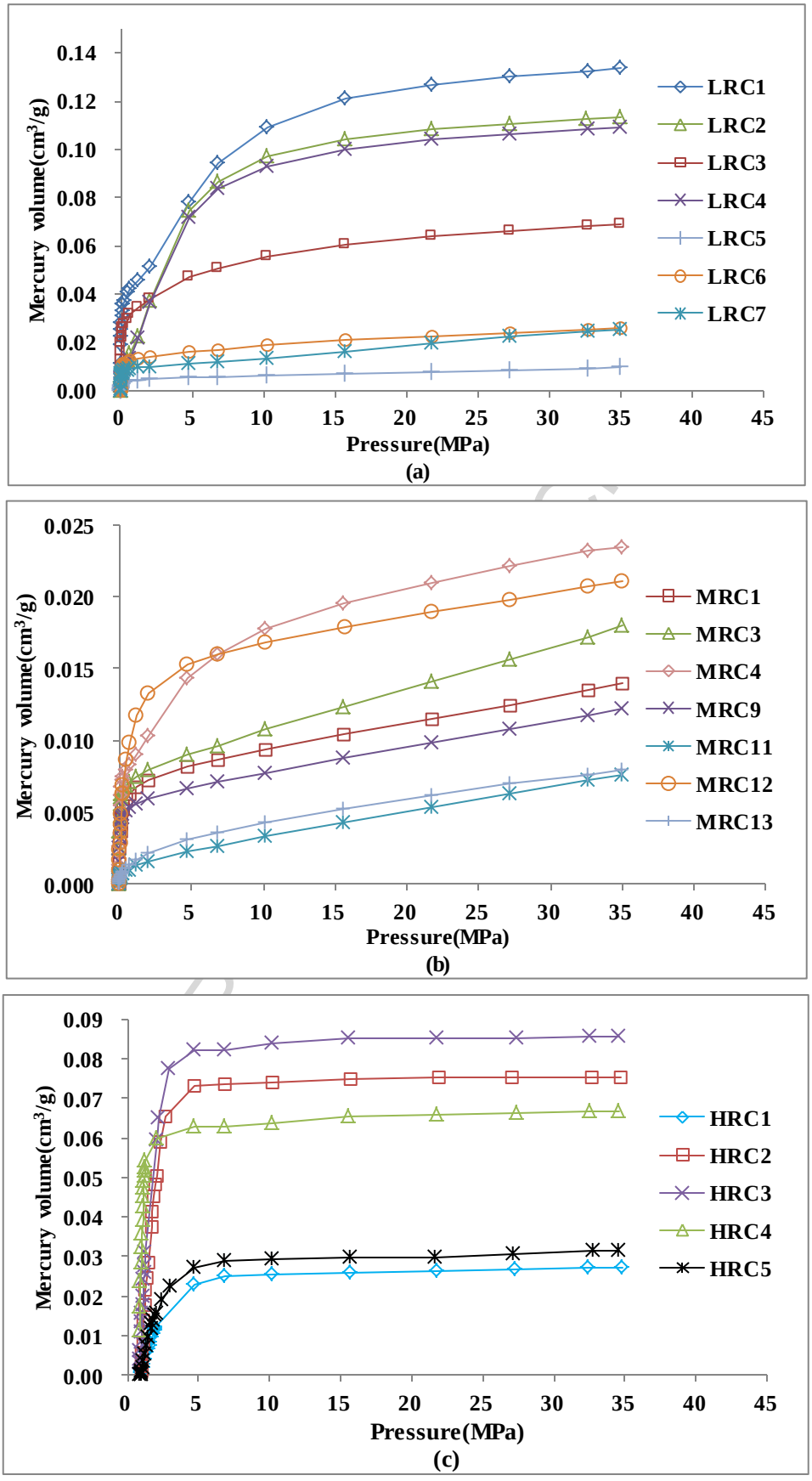

Fig. 1

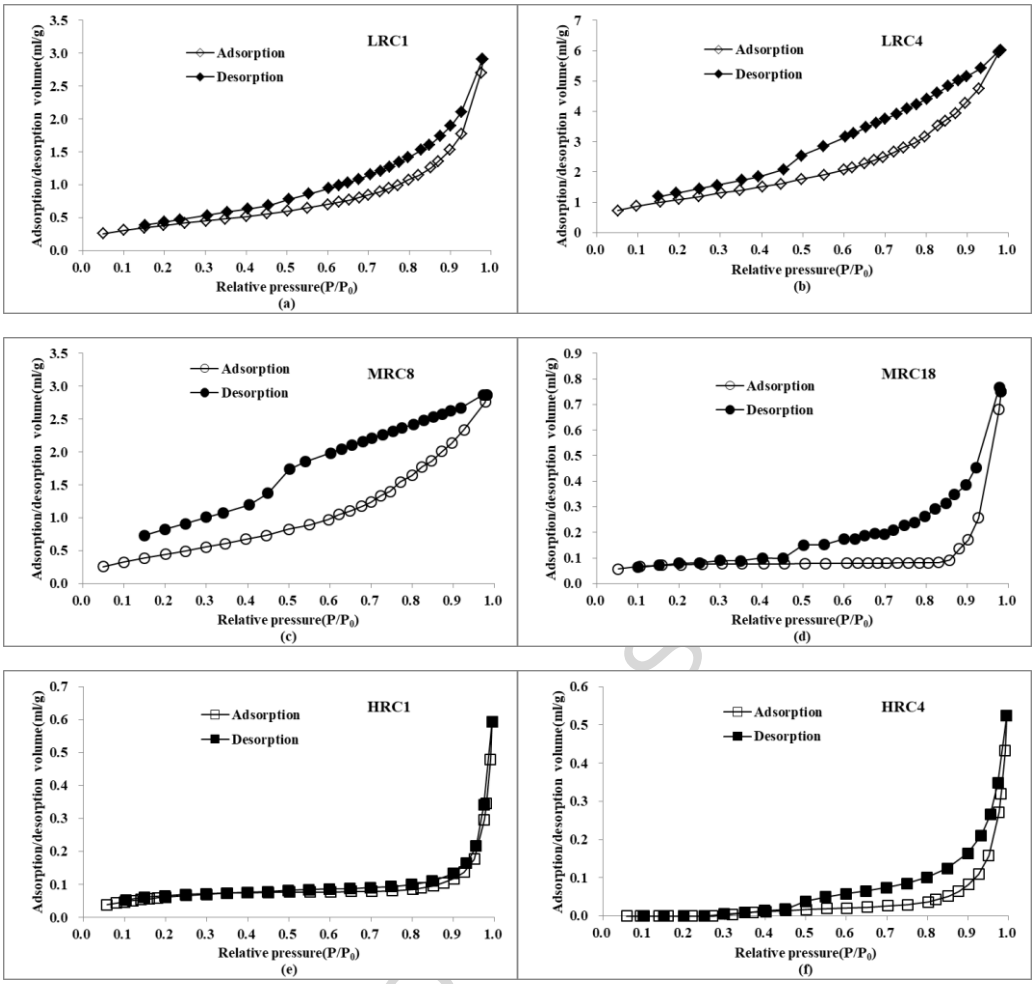

Fig. 2

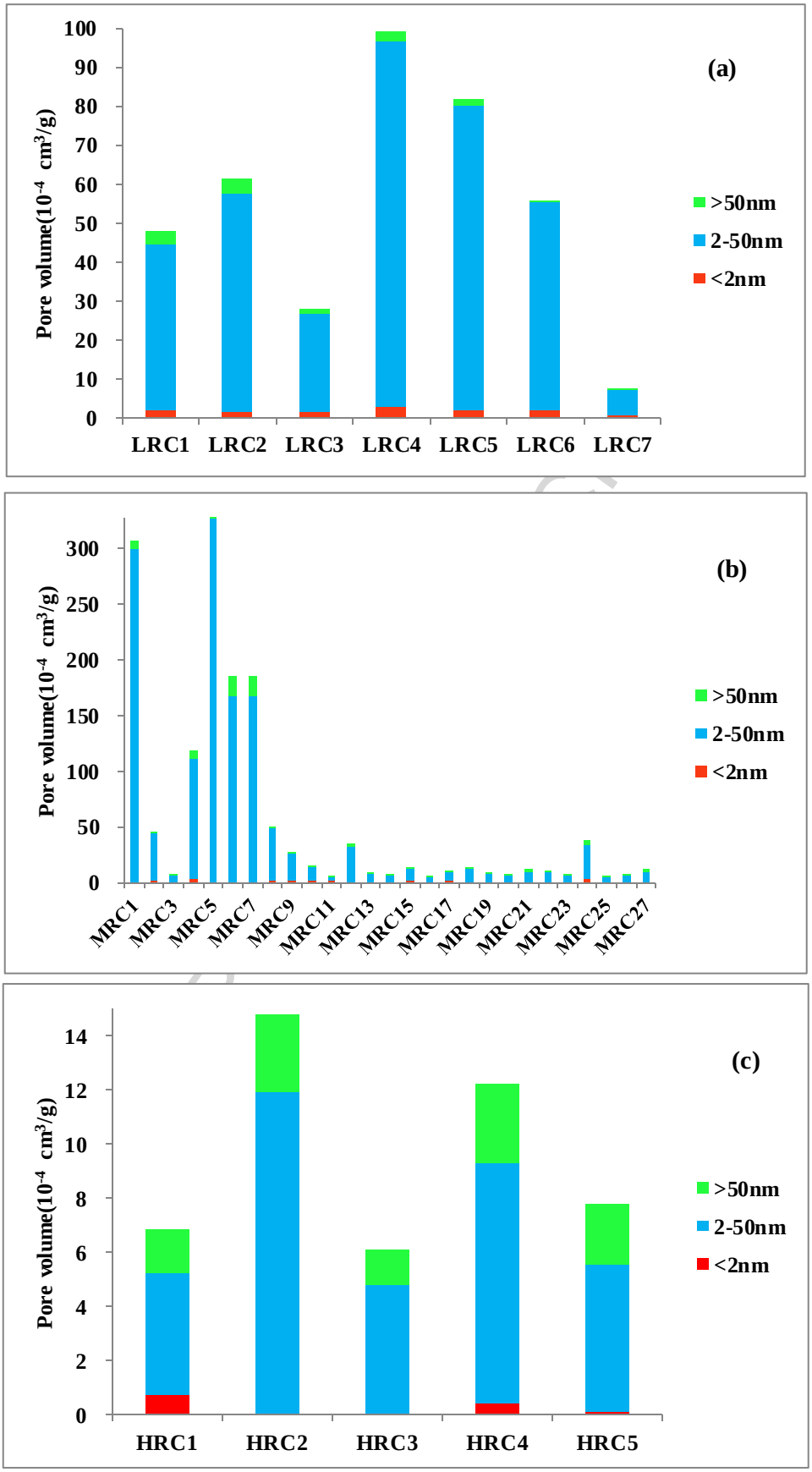

Fig. 3

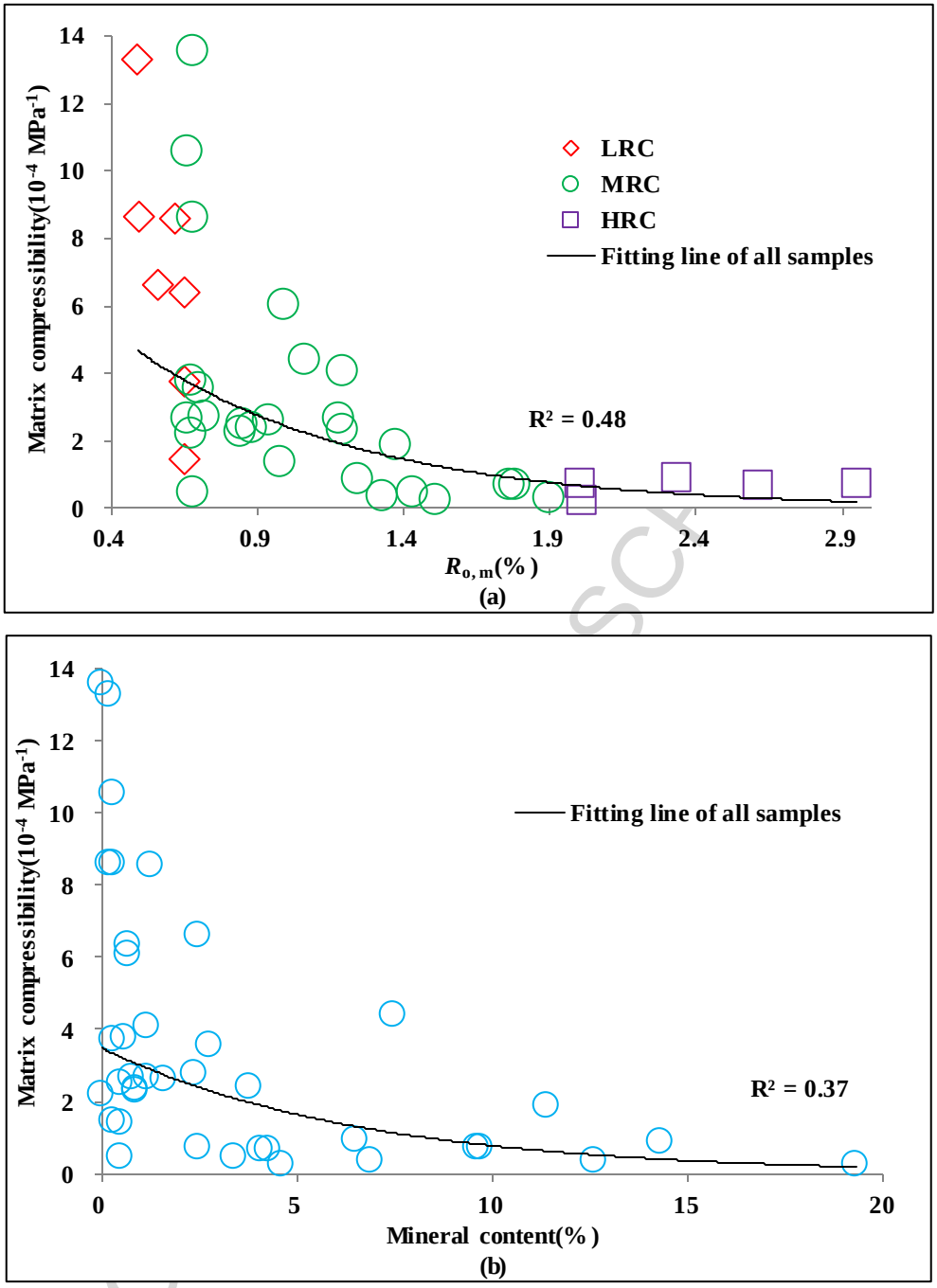

Fig. 4

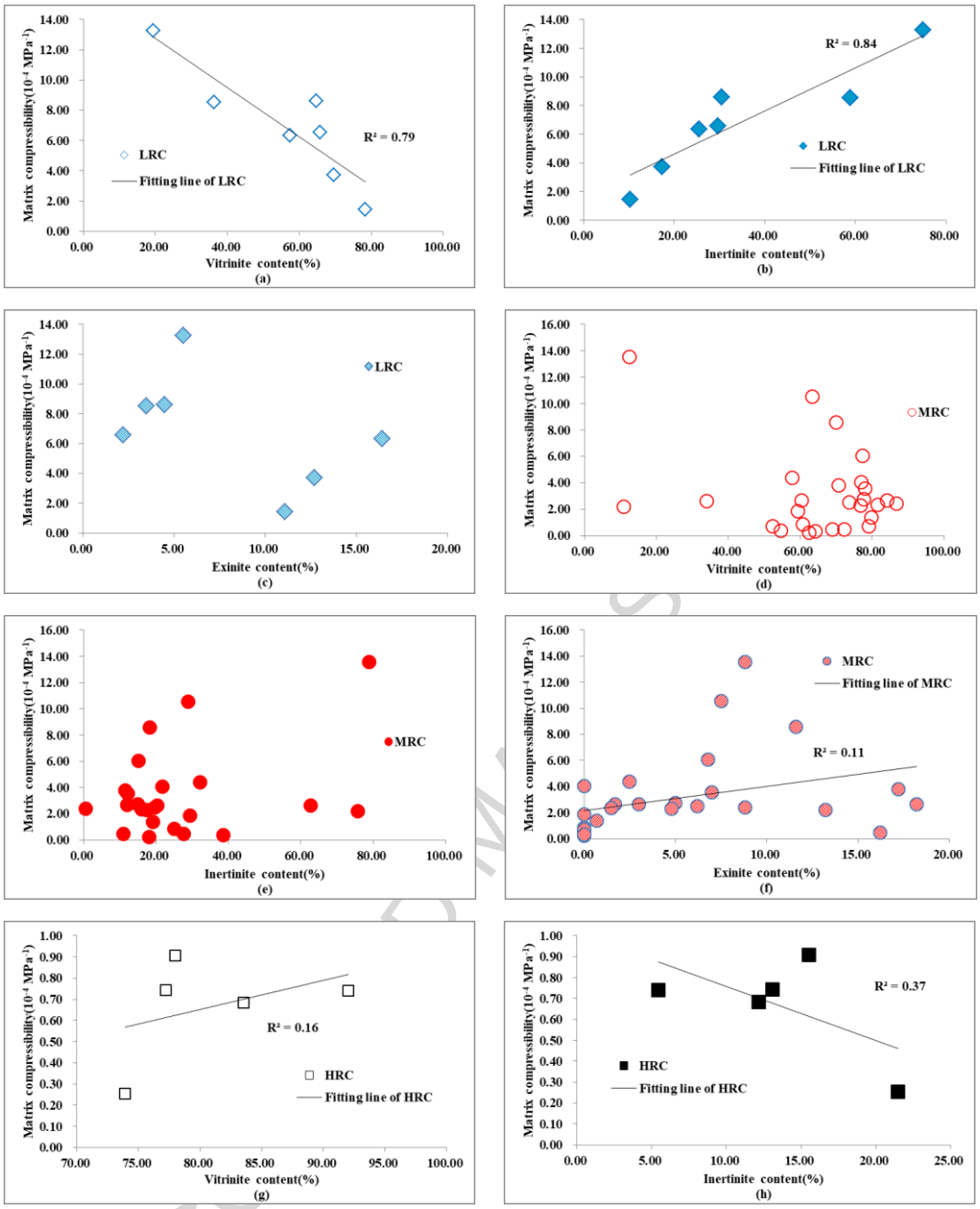

Fig. 5

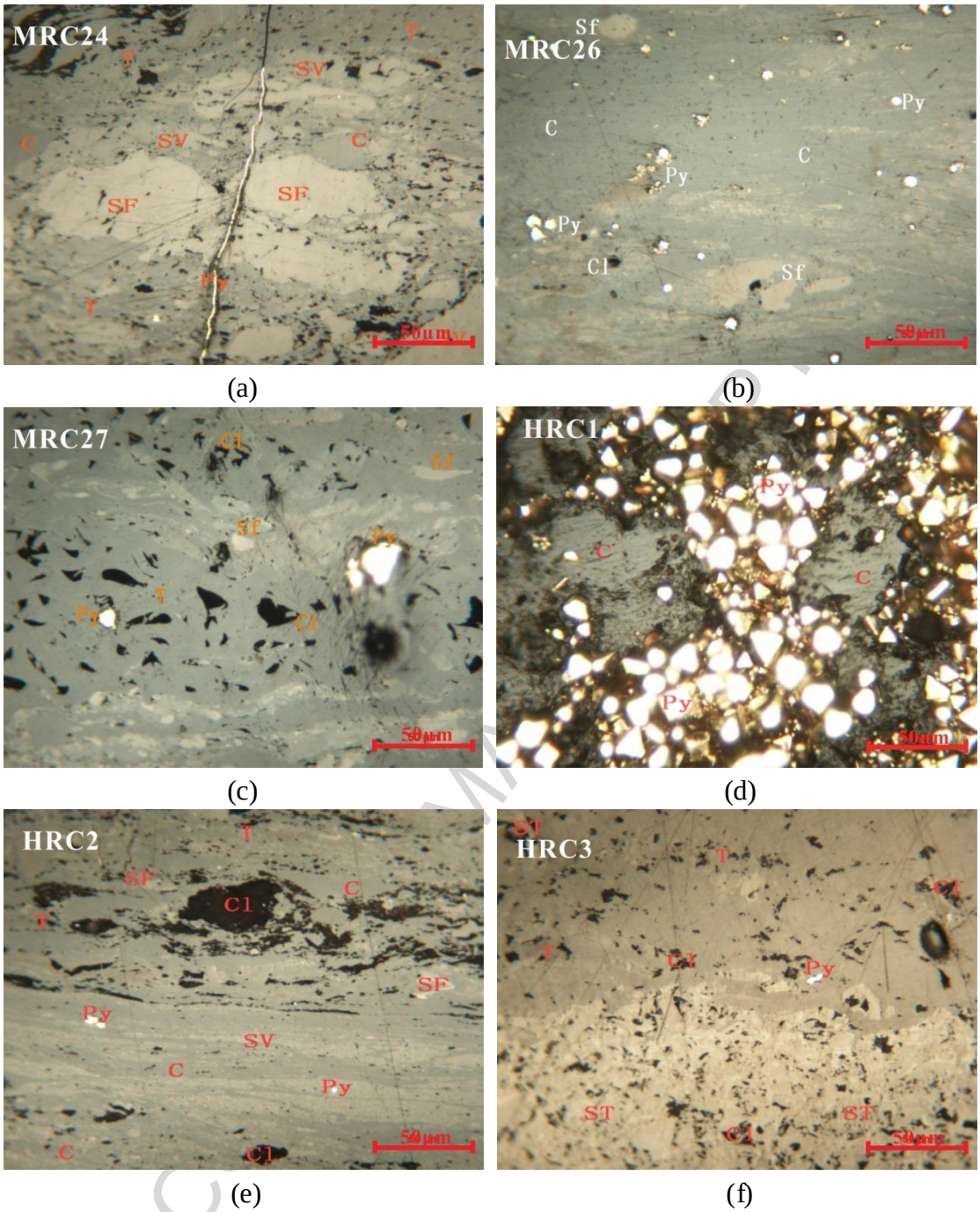

Fig. 6

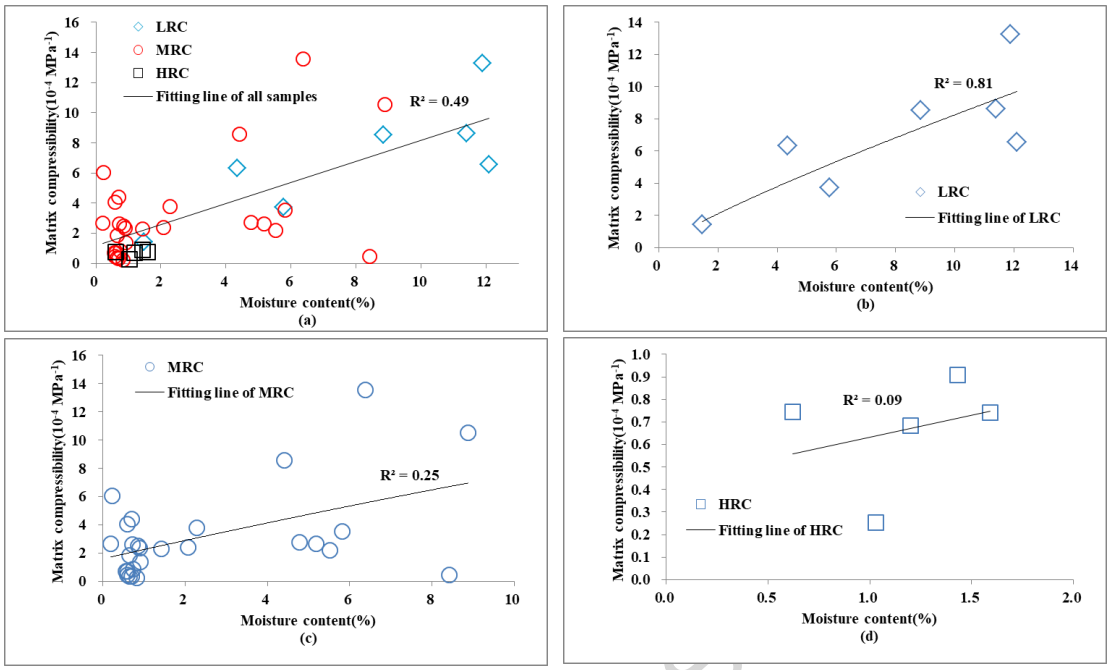

Fig. 7

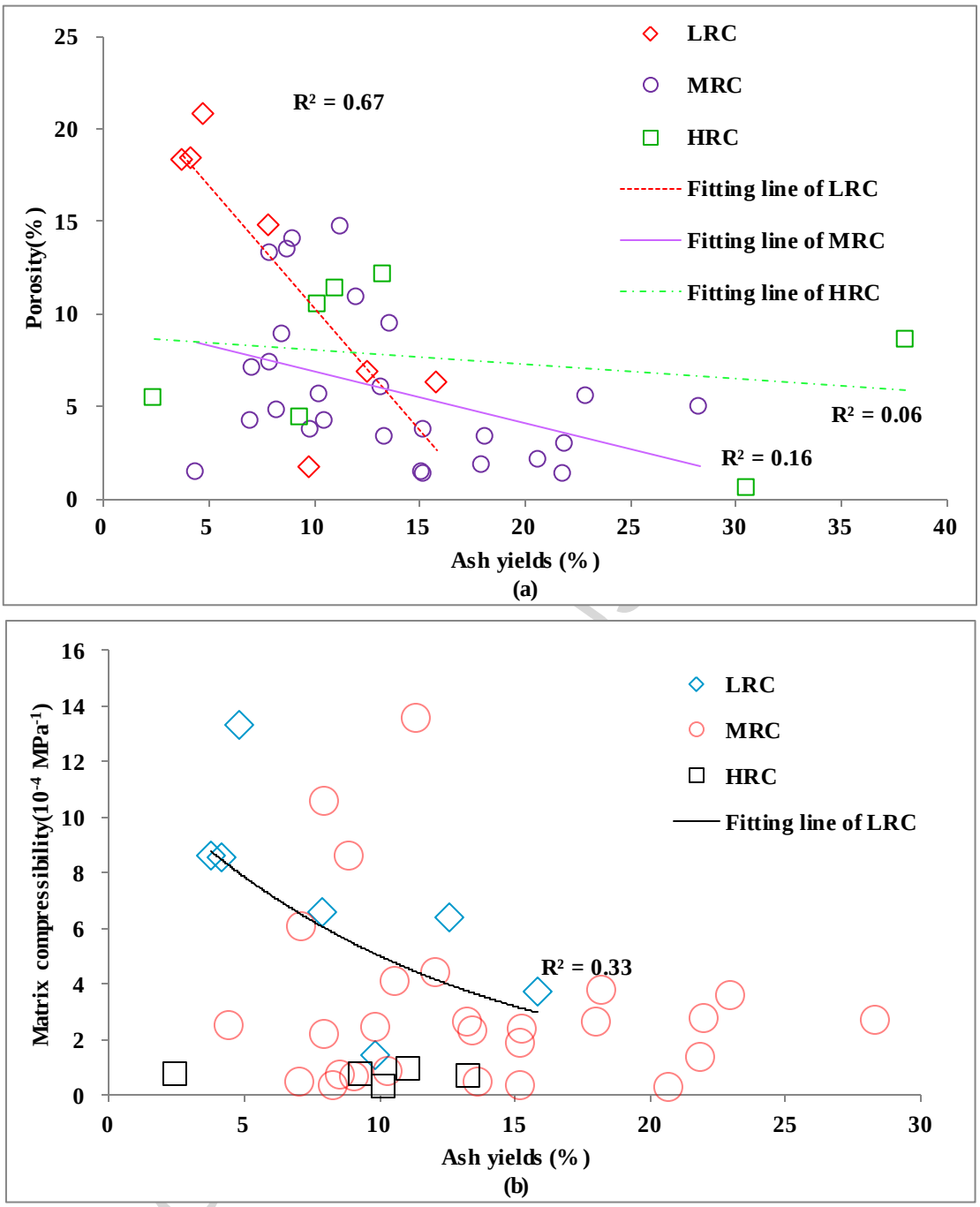

Fig. 8

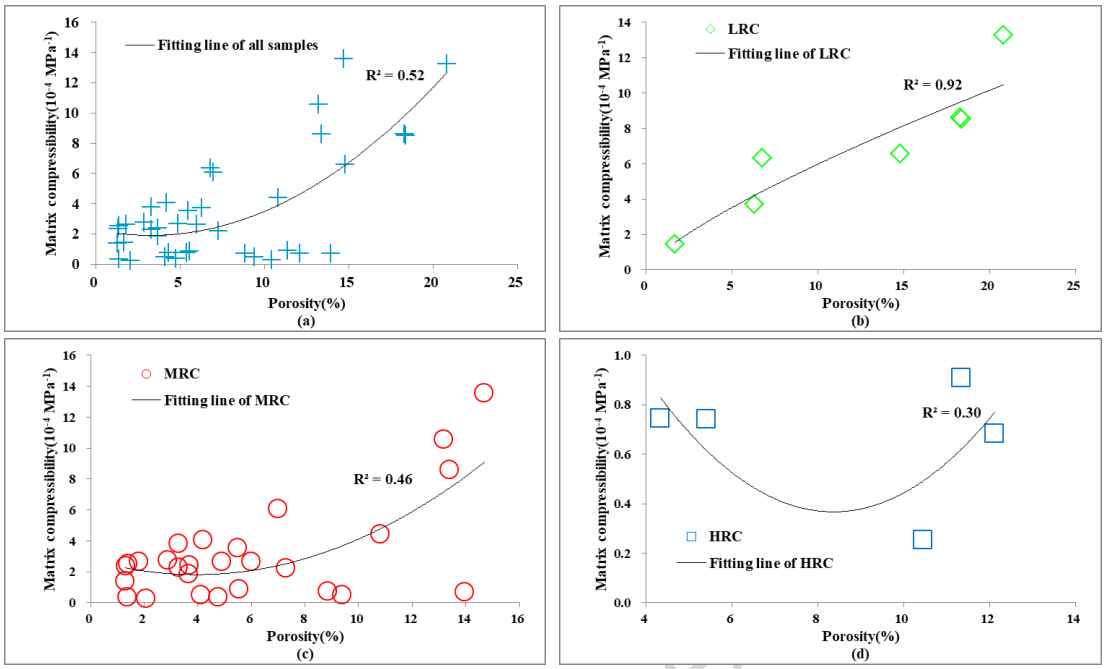

Fig. 9

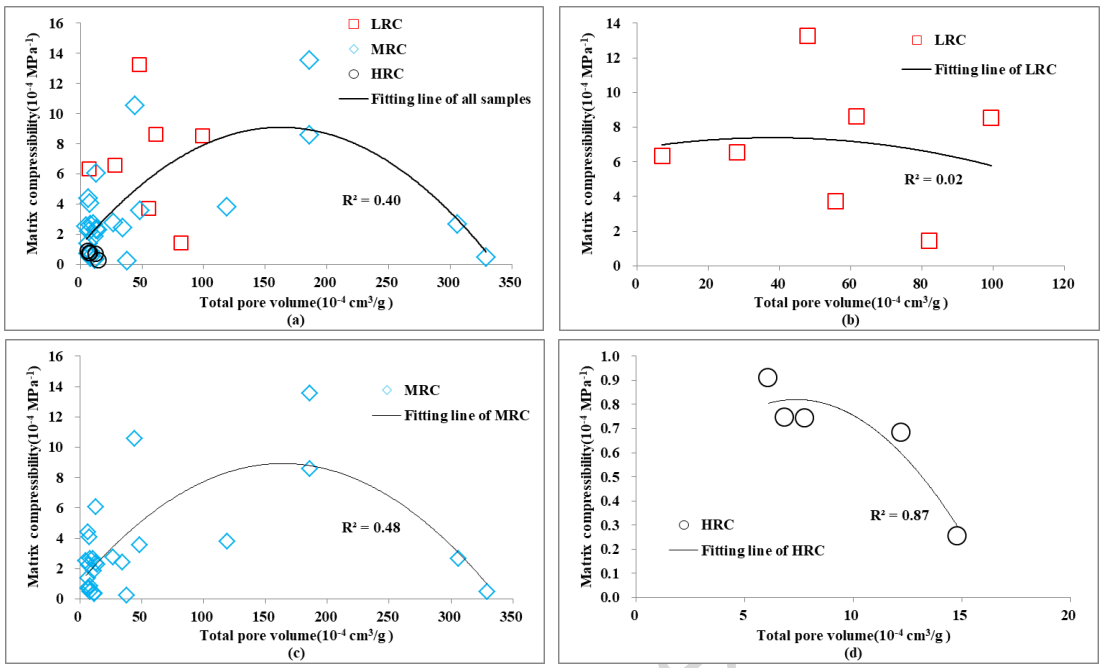

Fig. 10

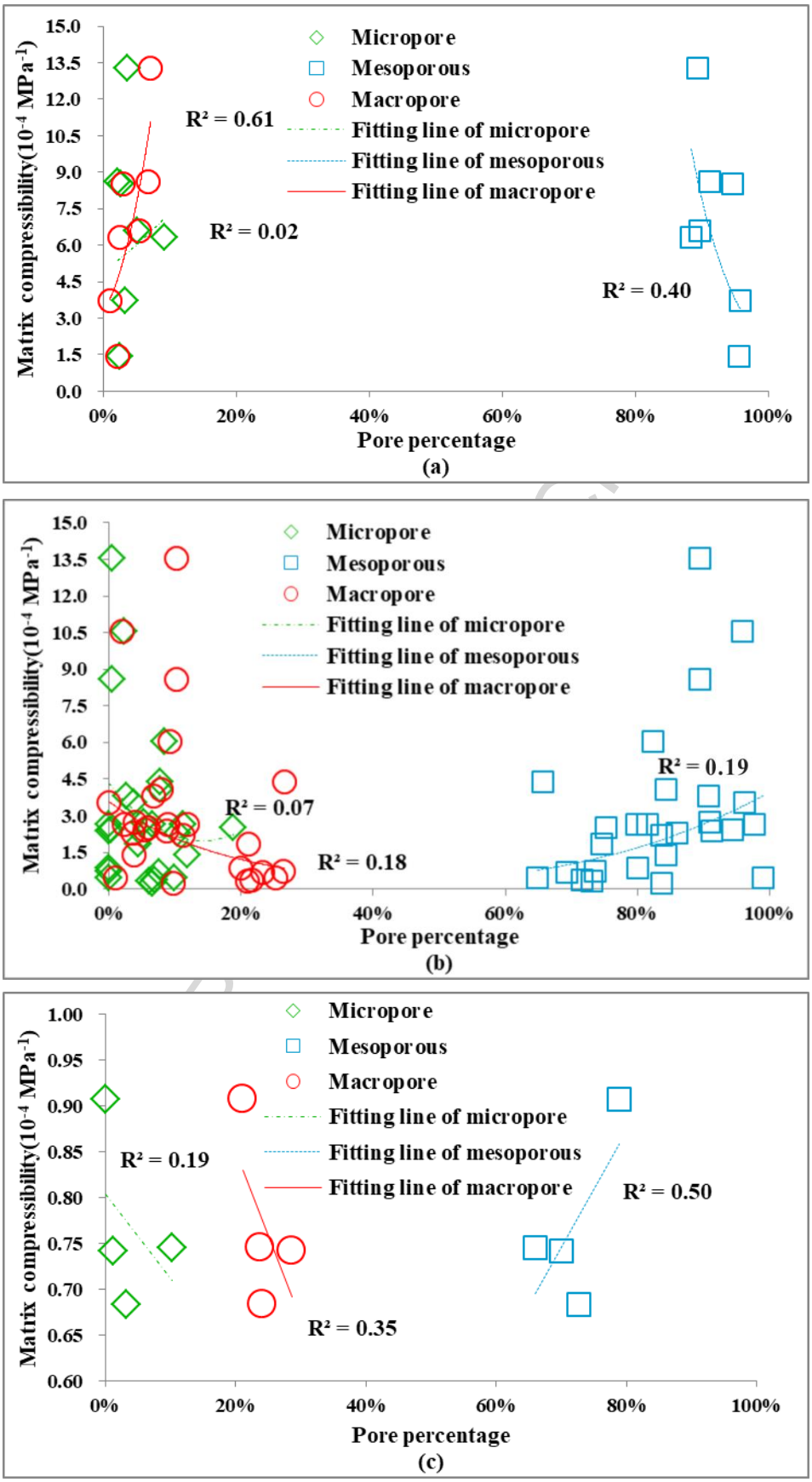

Fig. 11

Table 1 Sample information and basic parameters of the selected Chinese coals

Coal rank	Sample no.	Basins	$R_{o,m}$ (%)	Maceral and mineral (vol %)				Porosity (%)	Prox (wt %, ad)	
				V	I	E	M		Moisture	Ash yields
Low-rank Coal	LRC1	Junggar	0.49	19.40	74.90	5.50	0.20	20.80	11.88	4.78
	LRC2		0.50	64.70	30.50	4.50	0.30	18.30	11.39	3.77
	LRC3		0.56	65.70	29.60	2.20	2.50	14.80	12.1	7.9
	LRC4		0.62	36.40	58.80	3.50	1.30	18.40	8.84	4.15
	LRC5	Hegang	0.65	78.30	10.30	11.10	0.30	1.70	1.48	9.81
	LRC6	Junggar	0.65	69.60	17.40	12.70	0.30	6.30	5.78	15.82
	LRC7		0.65	57.40	25.50	16.40	0.70	6.80	4.35	12.56
Medium-rank Coal	MRC1	Junggar	0.66	63.40	28.80	7.50	0.30	13.20	8.88	7.95
	MRC2		0.66	60.30	20.30	18.20	1.20	6.00	5.18	13.25
	MRC3		0.67	11.00	75.80	13.20	0.00	7.30	5.52	7.94
	MRC4	Sanjiang	0.67	70.60	11.60	17.20	0.60	3.30	2.28	18.18
	MRC5		0.68	72.30	11.00	16.20	0.50	9.40	8.42	13.63
	MRC6		0.68	69.90	18.30	11.60	0.20	13.40	4.41	8.82
	MRC7	Junggar	0.68	12.40	78.80	8.80	0.00	14.70	6.38	11.30
	MRC8		0.70	78.00	12.20	7.00	2.80	5.50	5.82	22.95
	MRC9		0.72	77.60	15.00	5.00	2.40	2.90	4.78	21.96
	MRC10	Sanjiang	0.84	76.80	17.50	4.80	0.90	3.30	1.43	13.42
	MRC11	Hegang	0.85	73.70	19.60	6.20	0.50	1.40	0.86	4.41
	MRC12	Sanjiang	0.88	86.80	0.60	8.80	3.80	3.70	2.08	9.86
	MRC13	Hegang	0.94	34.00	62.70	1.70	1.60	1.80	0.72	18.00
	MRC14	Boli	0.98	79.70	19.10	0.70	0.50	1.30	0.92	21.81
	MRC15	Jixi	0.99	77.30	15.20	6.80	0.70	7.00	0.23	7.12
	MRC16	Ordos	1.06	57.81	32.19	2.50	7.50	10.83	0.71	12.04
	MRC17	Jixi	1.18	84.10	12.10	3.00	0.80	4.90	0.2	28.28
	MRC18	Boli	1.19	81.50	16.10	1.50	0.90	1.33	0.9	15.27
	MRC19		1.19	77.00	21.80	0.00	1.20	4.20	0.59	10.57
	MRC20		1.24	60.68	25.02	0.00	14.30	5.55	0.74	10.27
	MRC21		1.33	54.56	38.54	0.00	6.90	4.76	0.66	8.27
	MRC22	Ordos	1.37	59.27	29.33	0.00	11.40	3.68	0.66	15.19
	MRC23		1.43	68.97	27.63	0.00	3.40	4.13	0.59	7.03
	MRC24		1.51	62.54	18.16	0.00	19.30	2.07	0.83	20.67
	MRC25		1.76	52.25	38.15	0.00	9.60	8.86	0.56	8.54
	MRC26	Qinshui	1.78	79.02	16.88	0.00	4.10	13.96	0.6	9.03
	MRC27		1.90	64.15	23.25	0.00	12.60	1.38	0.71	15.18
High-rank Coal	HRC1	Qinshui	2.00	77.21	13.09	0.00	9.70	4.34	0.62	9.34
	HRC2		2.01	73.94	21.47	0.00	4.60	10.46	1.03	10.18
	HRC3		2.33	77.98	15.52	0.00	6.50	11.36	1.43	11.06
	HRC4		2.61	83.55	12.15	0.00	4.30	12.12	1.20	13.30
	HRC5		2.95	92.04	5.46	0.00	2.50	5.42	1.59	2.45

Note: ad- as received basis; V- Vitrinite; I - Inertinite; E- Exinite; M - Mineral; Prox- Proximate analysis.

Table 2 Calculation parameters of the coal matrix compressibility for different rank coals

Sample no.	$R_{o,m}$ (%)	V_m (cm^3/g)	N ($\times10^{-4}$)	PV ($\times10^{-4}$, cm^3/g)	C_m ($\times10^{-4}$, MPa^{-1})
LRC1	0.49	0.86	12.00	17.70	13.26
LRC2	0.50	0.86	8.00	15.90	8.61
LRC3	0.56	0.87	6.00	8.60	6.57
LRC4	0.62	0.88	8.00	15.10	8.53
LRC5	0.65	0.67	1.00	0.95	1.44
LRC6	0.65	0.75	3.00	5.70	3.72
LRC7	0.65	0.72	5.00	12.90	6.34
MRC1	0.66	0.78	10.00	49.00	2.64
MRC2	0.66	0.66	2.00	7.40	10.55
MRC3	0.67	0.73	3.00	39.00	2.20
MRC4	0.67	0.77	3.00	1.86	3.79
MRC5	0.68	0.73	3.00	75.00	0.47
MRC6	0.68	0.81	8.00	30.00	8.58
MRC7	0.68	0.76	13.00	75.00	13.56
MRC8	0.70	0.80	3.00	4.30	3.55
MRC9	0.72	0.68	2.00	3.60	2.74
MRC10	0.84	0.81	2.00	4.61	2.28
MRC11	0.85	0.79	2.00	0.77	2.51
MRC12	0.88	0.72	2.00	7.50	2.40
MRC13	0.94	0.71	2.00	3.51	2.63
MRC14	0.98	0.69	1.00	1.17	1.38
MRC15	0.99	0.80	5.00	4.70	6.05
MRC16	1.06	0.87	4.00	5.00	4.40
MRC17	1.18	0.72	2.00	2.51	2.66
MRC18	1.19	0.75	2.00	6.65	2.35
MRC19	1.19	0.72	3.00	1.68	4.06
MRC20	1.24	0.94	1.00	5.37	0.86
MRC21	1.33	0.87	0.60	8.07	0.36
MRC22	1.37	0.93	2.00	7.56	1.86
MRC23	1.43	0.97	0.70	6.80	0.47
MRC24	1.51	0.97	0.80	15.91	0.24
MRC25	1.76	0.98	0.90	5.97	0.71
MRC26	1.78	1.01	0.90	5.80	0.69
MRC27	1.90	1.03	0.60	7.39	0.33
HRC1	2.00	0.83	0.80	5.08	0.74
HRC2	2.01	0.86	0.60	10.78	0.25
HRC3	2.33	0.92	1.00	4.58	0.91
HRC4	2.61	0.95	1.00	9.88	0.68
HRC5	2.95	0.86	0.90	7.31	0.74

Note: V_m- coal matrix volume; C_m- coal matrix compressibility; PV- Pore volume

Table 3 The difference of pore volume (19-100nm) between MIP and N_2 adsorption methods

Coal rank	Sample no.	Pore Vol.(19-100nm) ($\times10^{-4}$, cm^3/g)		Difference ($\times10^{-4}$, cm^3/g)
		MIP	N_2 adsorption	
Low Rank Coal	LRC1	396.59	17.70	378.89
	LRC2	267.65	15.90	251.75
	LRC3	182.20	8.60	173.60
	LRC4	255.77	15.10	240.67
	LRC5	40.13	0.95	39.18
	LRC6	88.77	5.70	83.07
	LRC7	136.33	12.90	123.43
Medium Rank Coal	MRC1	52.85	7.40	45.45
	MRC2	281.02	49.00	232.02
	MRC3	83.79	39.00	44.79
	MRC4	74.89	1.86	73.03
	MRC5	97.36	75.00	22.36
	MRC6	243.19	30.00	213.19
	MRC7	372.44	75.00	297.44
	MRC8	83.10	4.30	78.80
	MRC9	50.83	3.60	47.23
	MRC10	69.19	4.61	64.58
	MRC11	49.99	0.77	49.22
	MRC12	51.31	7.50	43.81
	MRC13	43.68	3.51	40.17
	MRC14	40.64	1.17	39.47
	MRC15	148.51	4.70	143.81
	MRC16	126.55	5.00	121.55
	MRC17	71.84	2.51	69.33
	MRC18	53.78	6.65	47.13
	MRC19	89.10	1.68	87.42
	MRC20	36.23	5.37	30.86
	MRC21	27.53	8.07	19.46
	MRC22	42.84	7.56	35.27
	MRC23	20.14	6.80	13.35
	MRC24	22.92	15.91	7.00
	MRC25	26.54	5.97	20.57
	MRC26	28.38	5.80	22.58
	MRC27	18.20	7.39	10.81
High Rank Coal	HRC1	21.34	5.08	16.26
	HRC2	16.62	10.78	5.85
	HRC3	34.00	4.58	29.42
	HRC4	40.64	9.88	30.77
	HRC5	25.84	7.31	18.52

Research Highlights

- Coal matrix compressibility shows an exponential decrease with increasing coal rank.
- An antithetical relation between inertinite and coal matrix compressibility.
- The wetting action of water molecules weakens the link between coal particles.
- Mineral appearance has significant impact on coal matrix compressibility.